

Disk heating agents across the Hubble sequence[★]

J. Gerssen^{1†}, K. Shapiro Griffin²

¹*Leibniz-Institut für Astrophysik Potsdam, An der Sternwarte 16, 14482 Potsdam, Germany.*

²*Space Sciences Research Group, Northrop Grumman Aerospace Systems, Redondo Beach, CA, USA*

18 October 2018

ABSTRACT

We measure the shape of the velocity ellipsoid in two late-type spiral galaxies (Hubble types Sc and Scd) and combine these results with our previous analyses of six early-type spirals (Sa to Sbc) to probe the relation between galaxy morphology and the ratio of the vertical and radial dispersions. We confirm at much higher significance (99.9 percent) our prior detection of a tight correlation between these quantities. We explore the trends of the magnitude and shape of the velocity ellipsoid axes with galaxy properties (colour, gas surface mass density, and spiral arm structure). The observed relationships allow for an observational identification of the radial and vertical disk heating agents in external disk galaxies.

Key words: galaxies: kinematics and dynamics – galaxies: individual: NGC 2280, NGC 3810 – galaxies: structure – galaxies: fundamental parameters

1 INTRODUCTION

More than half of the stellar mass in the local Universe is observed to reside in disk galaxies (Driver et al. 2007; Weinzirl et al. 2009), yet the evolutionary history of these systems remains poorly understood. Simulations of galaxy formation tend to produce spiral galaxies with most of their stellar mass fraction in a bulge component, and a direct comparison between observations and these simulations is usually not straightforward (Scannapieco et al. 2010). However, increasingly powerful simulations of disk galaxy formation are reaching a stage where internal dynamical properties, such as rotational and random velocities, can also be investigated and compared to observations (Scannapieco et al. 2011). These velocity distribution functions are fossil relics of the history of gravitational forces acting on stars and therefore of the evolutionary histories of spiral galaxies; for this reason, measurement of the stellar velocity distributions in local spiral galaxies is an important tool for probing the evolution of these systems.

From observations in the solar neighbourhood it has been shown that the random motions of thin disk stars correlates with their ages, the age- σ relation (Wielen 1977; Binney et al. 2000). This relation is most commonly parametrized as a power law of the form $\sigma \propto t^\alpha$, with existing measurements of α spanning the range of 0.2 – 0.5 (see e.g. Nordström et al. 2004 for results from the Geneva-

Copenhagen survey). However, the age- σ relation has also been interpreted as saturating at a constant dispersion after ~ 5 Gyr (e.g. Carlberg et al. 1985; Seabroke & Gilmore 2007; Soubiran et al. 2008) or as several discrete increases in velocity dispersion (Quillen & Garnett 2001). As a result of the observational uncertainty, it is not straightforward to identify the disk heating mechanism responsible for the rise in velocity dispersions.

Additional constraints on the disk heating mechanism are provided by the three-dimensional distribution of stellar velocity dispersions, whose magnitude and direction designate the axes of an ellipsoid; this trivariate Gaussian function was originally proposed by Schwarzschild (1907). The so-called velocity ellipsoid is parameterized by its two axis ratios, σ_ϕ/σ_R and σ_z/σ_R . In an axisymmetric disk with stellar orbits not too far from circular (the epicycle approximation), σ_ϕ/σ_R depends only on the circular velocity and not on any disk heating mechanism. Measurements of the ratio σ_z/σ_R can thus be used to probe the velocity distribution and therefore to constrain the heating processes in galactic disks.

In the Milky Way, the age- σ relation and velocity ellipsoid shape ($\sigma_z/\sigma_R = 0.5$) have been studied extensively, and a number of heating mechanisms have been proposed to simultaneously explain the observations. These include encounters with giant molecular clouds (GMCs, Spitzer & Schwarzschild 1951; Lacey 1984; Lacey & Ostriker 1985), perturbations from irregular and transient spiral structure Barbanis & Woltjer 1967; Jenkins & Binney 1990; Fuchs 2001; Minchev & Quillen 2006), perturbations from stellar bars (Saha et al. 2010), dissolution of young stellar clusters (Kroupa 2002),

[★] Based on observations made with ESO Telescopes at the La Silla Observatory under programmes 074.B-0550(A) & 078.B-0152(A).

[†] E-mail: jgerssen@aip.de

scattering by dark halo objects or globular clusters (Hänninen & Flynn 2002; Vande Putte et al. 2009), and disturbances by satellite galaxies or minor mergers (Velazquez & White 1999). This plethora of disk heating theories reflects the limited constraints provided by measurements in a single galaxy. However, many of these theories are implicitly dependent on galaxy morphology; progress towards an understanding of secular evolution in disk galaxies therefore critically depends on data from external galaxies spanning a range of Hubble types.

The numerical study of Jenkins & Binney (1990) is one of the few that can be directly compared with observations of disk heating in external galaxies. This theory combines two disk heating mechanisms, spiral transients and GMCs, in what appears to be the simplest explanation that is consistent with most of the observations. By varying the relative importance of the two mechanisms they showed that disk heating, as quantified by the ratio σ_z/σ_R , decreases with the increase of spiral strength, e.g. along the Hubble sequence (but see also Sellwood 2008).

We have developed a technique (Gerssen et al. 1997) to measure the velocity dispersion ratio in galaxies from spectra obtained along the major and minor axis. We applied this technique to six disk galaxies spanning a range in Hubble type from Sa to Sbc (Gerssen et al. 1997, 2000; Shapiro et al. 2003). In each system we were able to constrain σ_z/σ_R by averaging measurements over radii in the range of one to two disk scale lengths. While the uncertainties on these ratios are large for individual galaxies, there appears to be a trend with Hubble type that is consistent with the predictions of Jenkins & Binney (1990). However, the applicability of this trend to later-type systems remained unclear (Shapiro et al. 2003).

In this paper, we address this issue by directly measuring the velocity ellipsoid ratios in two late-type disk galaxies: NGC 3810 (Sc) and NGC 2280 (Scd). Section 2 presents our observations of these galaxies. Section 3 describes our kinematic extraction and modeling procedure. Section 4 presents our derived velocity ellipsoid ratios and combines these results with our previous work on early-type disks to examine the ratio of vertical to radial velocity dispersions across the Hubble sequence. The new results are consistent with the trend observed earlier and suggest that the relative effectiveness of vertical to radial secular evolution processes diminishes as a function of galaxy morphology. We additionally combine our data with literature measurements of the velocity ellipsoid in elliptical and lenticular galaxies (Cappellari et al. 2007) to reveal intriguing trends across all galaxy morphologies. In Section 5, we use our results to identify heating agents at work in spiral galaxies, and in Section 6, we conclude.

2 OBSERVATIONS & DATA REDUCTION

2.1 Spectroscopy

To probe the shape of the velocity ellipsoid at the end of the Hubble sequence, we obtained long-slit spectra along the major and minor axes of two late-type spiral galaxies. The galaxy properties are listed in Table 1, and the observing log is given in Table 2. All spectra were obtained with the EMMI

Table 1. Galaxy properties

Name	Type	Redshift (km s ⁻¹)	<i>i</i> (deg)	Scale length (arcsec)	Reference
NGC 2280	Scd	1899	64	19	1, 2
NGC 3810	Sc	993	32	16	1, 3

- 1) Redshifts and morphological classifications are from NED.
- 2) Scale length and inclination are derived in section 2.2.
- 3) Scale length and inclination are from Knapen et al. (2003).

Table 2. Observing log

Galaxy	Position angle (deg)	T_{exp} (min)	Date
NGC 2280			
Major axis	-22	156	Feb 2005
Minor axis	-112	160	Nov 2006
NGC 3810			
Major axis	25	210	Feb 2005
Minor axis	115	180	Feb 2005

spectrograph on the NTT during two runs in February 2005 and November 2006. We used the red medium dispersion grating (#6) to study the wavelength range 4800 - 5500 Å, which covers key interstellar emission ([OIII], H β) and stellar absorption (Mg *b*, several Fe) features. The slit length was 300'', and the slit width was 1'', resulting in a spectral resolution of 0.4 Å (~ 23 km s⁻¹). Measurements of the widths of unresolved arc lines in our calibration spectra are consistent with this value.

Observations were taken in exposures of either 1200s or 2400s, which were interspersed with calibration exposures of a He+Ar lamp. In addition, we obtained spectra of several stars of spectral types G0 III through K3 III, for use in extracting the stellar kinematics in our sample galaxies (§ 3.1); these stars are the dominant component in the Mg *b* and Fe stellar absorption features of spiral galaxies. To distribute the light from the template stars relatively uniformly on the detector and to prevent overexposure, the telescope was defocused during the observations of these stars.

Preliminary reduction steps (bias subtraction, flat-fielding) were done with our own IDL scripts, customized for EMMI data, and subsequent reduction steps (wavelength calibration, coadding individual exposures, extraction of 1-dimensional stellar spectra) were performed using standard IRAF¹ packages. For the kinematic analysis, we interpolate the spectral axis to logarithmic units in wavelength (linear in velocity) and spatially bin each galaxy spectrum to a minimum signal-to-noise (S/N) ratio of 10.

¹ IRAF is distributed by the National Optical Astronomy Observatory, which is operated by the Association of Universities for Research in Astronomy (AURA) under cooperative agreement with the National Science Foundation.

2.2 Photometry

Since the quantities of interest are properties of the galaxy disks and not of their bulges, we use broad-band images to measure the radii at which the disk dominates the stellar surface brightness. At these radii, the derived kinematics probe the disk stars and not the bulge and/or bar; we therefore limit our analysis (see § 3.2) to these radii.

For NGC 3810, Knapen et al. (2003) have measured the disk scale length to be $16''$ and the disk to dominate the galaxy light at $r > 5''$. For NGC 2280, we use an archival H -band image (Eskridge et al. 2002), obtained with the CTIO 1.5m telescope and available via the NED extragalactic database. We fit this image with the IRAF task ELLIPSE and derive an inclination of 64 degrees (from the best-fit axis ratios) and the surface brightness profile shown in Figure 1. The best-fit exponential disk model to this profile has a scale length of $19''$ and dominates the galaxy light at $r > 10''$. (Using a K -band image, Kassin et al. (2006) derive a scale length of 27 arcsec.) The radial surface brightness profile (Figure 1) hints at the presence of a small bar in NGC 2280. Between the linear behaviour of the surface brightness profile at large radii (the exponential disk) and the inner bulge profile, there is a distinct third component. This component dominates the surface brightness profiles at radii of $5\text{--}10''$; the combined shape of the surface brightness profile and flat minor axis velocity dispersions (see § 4.1) at these radii are consistent with the presence of a bar (e.g. Prieto et al. 2001; Gerssen et al. 2003).

3 ANALYSIS

3.1 Stellar and Gas Kinematics

For each binned spectrum, we extract the stellar kinematics using the *ppxf* method developed by Cappellari & Emsellem (2004). We modeled the absorption line kinematics from our galaxy spectra as convolutions of a template stellar spectrum with line-of-sight velocity distributions (LOSVD); the observation of the template stars with the same instrumental set-up as the galaxies allows the instrumental broadening to drop out during this fitting. Given the relatively low S/N of our data, we did not attempt to fit higher order moments of the LOSVD (e.g. h_3, h_4 , etc) and instead assumed the LOSVD to be Gaussian. Since the outer disks of late-type galaxies are faint and the spectra are dominated by sky emission, we employ the method of Weijmans et al. (2009), in which a median sky spectrum taken from the edge of our long-slit is included as a template in the fitting procedure. We extract the stellar kinematics using several GIII and KIII templates. An optimal combination of these templates did not significantly improve the results, so we chose the K1III giant HD114971, which yields marginally better χ^2 , to extract the stellar kinematics in both galaxies.

The derived stellar velocities and velocity dispersions along the major and minor axes of our sample galaxies are presented in Figure 2. In these plots, the abscissa is the radius in the plane of the disk, which for the minor axes was obtained through deprojection. The velocity dispersion profiles for both galaxies show central drops. This is a fairly common phenomenon (e.g. Comerón et al. 2008) and is usually attributed to a central disk or nuclear bar. These central

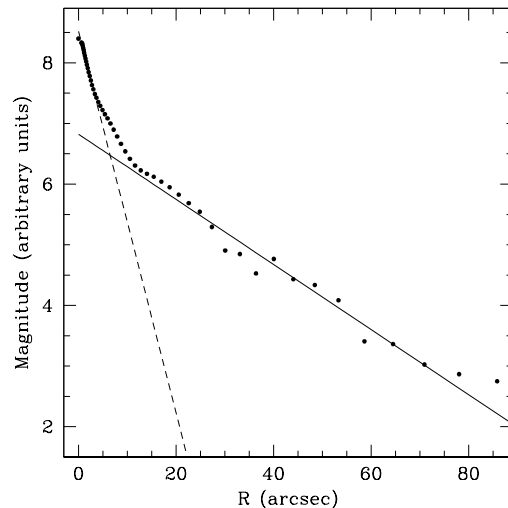


Figure 1. The radial surface brightness profile of NGC 2280 derived from an archival H -band image obtained with the CTIO 1.5m telescope (Eskridge et al. 2002). The best-fit exponential model to the outer disk (solid line) has an exponential scale length of $19''$. The dashed line is a guide (not a fit) delineating the bulge component. The presence of a third component, perhaps a small bar, can be inferred from the excess of light between 5 and 10 arcsec.

velocity dispersion drops do not affect the results presented in this paper as their influence is confined to radii that we exclude from our analysis.

To probe the circular velocity in our target galaxies we use the [OIII] emission line at 5007 \AA . We fit this line in each spatial bin with a Gaussian profile to derive the best-fit centroids. As the lines are unresolved in our data (width $< 23 \text{ km s}^{-1}$) we do not attempt to quantify the gas velocity dispersions. In the following, we assume the measured gas velocities to be a good approximation of the circular velocity in our galaxies.

3.2 Modeling

To measure the velocity ellipsoid in our late-type galaxies, we model the stellar and gas kinematics using the method developed by Gerssen et al. (1997) and subsequently applied to a larger range of morphological types by Gerssen et al. (2000) and Shapiro et al. (2003).

Briefly, the line-of-sight (los) kinematics along the major and minor axes of intermediate inclination galaxies probe different projections of the velocity ellipsoid, namely σ_ϕ and σ_R along the major axis and σ_R and σ_z along the minor axis:

$$\sigma_{\text{major}}^2 = \sigma_R^2 \sin^2 i + \sigma_z^2 \cos^2 i \quad (1)$$

$$\sigma_{\text{minor}}^2 = \sigma_\theta^2 \sin^2 i + \sigma_z^2 \cos^2 i \quad (2)$$

The epicycle approximation (e.g. Eq. 2 in Shapiro et al. 2003) for stellar orbits in a disk yields σ_ϕ/σ_R as a function of only the circular velocity $V_c(R)$ of the system. Assuming axisymmetry, measurements of σ_{los} along the major and minor axes and of V_c along the major axis fully constrain the shape of the velocity ellipsoid. Including the stellar ro-

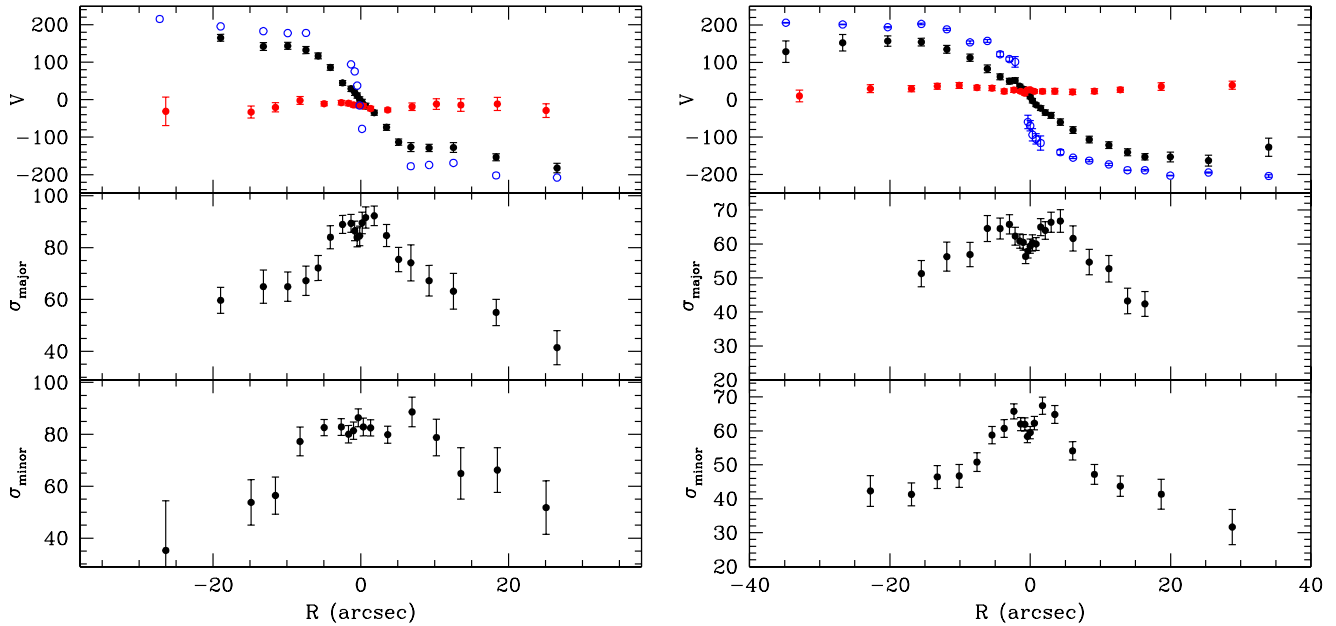


Figure 2. Observed kinematics of the two late-type spiral galaxies, **left:** NGC 2280 (type Scd) and **right:** NGC 3810 (type Sc). In all panels the kinematic information is given in km s^{-1} . Filled circles represent major and minor axis stellar data; open circles represent gas data. Error bars for the stellar velocities are shown but are generally smaller than the plot symbols. The top panel for each galaxy shows the gas major axis rotation curve (blue open circles), the stellar major axis rotation curve (black filled circles), and the stellar minor axis velocities overplotted (red filled circles, roughly constant at 0 km s^{-1}). The galaxy systemic velocities have been subtracted. The lower two panels for each galaxy show the major and minor axis stellar velocity dispersions respectively. The abscissa is the radius in the disk, which, for the minor axis, was obtained through deprojection.

tation curve $\bar{V}(R)$ and modeling the asymmetric drift as a function of only the disk scale length and σ_R (i.e. assuming no tilt σ_{Rz} to the velocity ellipsoid; see Gerssen et al. 1997) then overdetermines the system and provides an additional constraint to the model:

$$\bar{V}^2 = V_c^2 - \sigma_R^2 \left[\frac{R}{h} - R \frac{\partial}{\partial R} \ln(\sigma_R^2) - \frac{1}{2} + \frac{R}{2V_c} \frac{\partial V_c}{\partial R} \right] \quad (3)$$

For a more detailed description of this method the reader is referred to Shapiro et al. (2003). In practice, the low intrinsic luminosity and small velocity dispersion of our late-type galaxies (compared to the early-type disks studied by Gerssen et al. 1997, 2000; Shapiro et al. 2003) resulted in only a few data points sampling the radial behavior of the kinematic profiles. This paucity of data points forced us to include the emission line kinematics directly in the modelling rather than use them as an independent check on the best-fit results in our previous analyses.

The four observables (σ_{major} , σ_{minor} , V_c , and \bar{V}) are simultaneously fit to produce $\sigma_z(R)$, $\sigma_R(R)$, and $V_c(R)$. The velocity dispersions as a function of radius are assumed to be exponentially declining with identical scalelength h_{kin} , parametrized by $\sigma_{z,0}$, $\sigma_{R,0}$, and h_{kin} , and the circular velocity is assumed to be a power law with radius, described by $V_{c,0}$ and power-law index α , for a total of five fitted parameters.

As our data set is rather small with fairly large error bars on each point, we employ two parameter space minimization techniques: the Levenberg-Marquardt method and a simulated annealing method. In both cases we follow the

Table 3. Best-fit model parameters

Parameter	NGC 2280	NGC 3810
$V_{c,0}$ (km s^{-1})	92 ± 21	142 ± 15
α	0.26 ± 0.07	0.11 ± 0.04
$\sigma_{R,0}$ (km s^{-1})	126 ± 29	183 ± 24
$\sigma_{z,0}$ (km s^{-1})	31 ± 24	54 ± 22
h_{kin} (arcsec)	54 ± 48	22 ± 3
σ_z/σ_R	0.25 ± 0.20	0.29 ± 0.12

implementation of these method as described in Press et al. (1992). Both methods fit our data equally well in a χ^2 sense. The resulting best-fit models are overplotted on the data in Figure 3 and described in Table 3.

The complexity of the dynamical modeling renders direct error propagation not straightforward in our analysis. We estimate the confidence limits using 500 Monte-Carlo realizations of the original data set. We analyze each realization using both χ^2 minimization techniques and find that they yield similar estimates of the uncertainties.

4 RESULTS

4.1 NGC 2280

The Scd galaxy NGC 2280 is the latest Hubble type in our full sample of galaxies with measured velocity ellipsoid axis ratios. Kinematic data at radii less than 10 arcsec are dominated by the bulge and bar components in this system

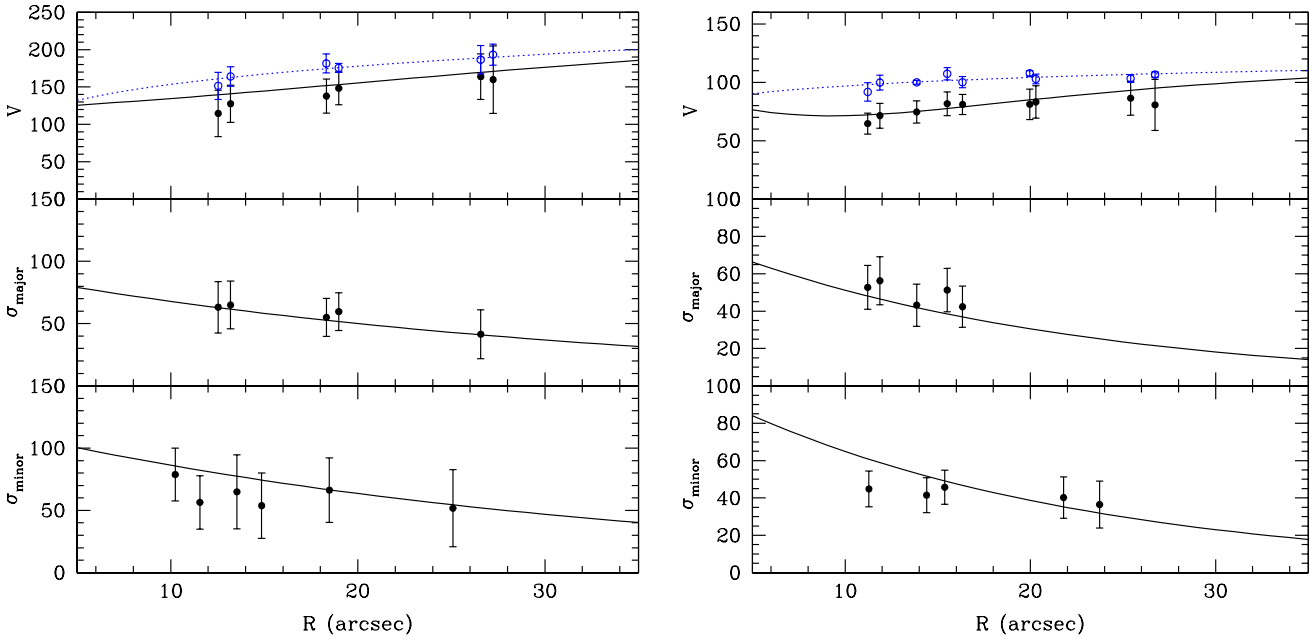


Figure 3. Similar to Fig. 2 but showing the observed kinematic quantities at absolute radii and excluding data contaminated by bulge light, **left:** NGC 2280 and **right:** NGC 3810. All kinematic quantities (filled circles: stars, open circles: gas) are in km s^{-1} . The best-fit models to the observed stellar kinematics (Eq. 3, 1 and 2 respectively from top to bottom) are shown as solid lines. Unlike our previous study (Shapiro et al. 2003), where the gas velocities were used as a consistency check on the circular velocities (dotted lines), we include the gas velocities directly in our fitting procedure to better constrain the velocity ellipsoids in these later-type disk galaxies.

and are therefore excluded from the analysis. The remaining dataset is limited in its extent but sufficient to derive a best-fit model, albeit with large uncertainties. The kinematic scale length parameter, in particular, has a large uncertainty. However, this parameter drops out of the primary quantity of interest, the ratio of the vertical to radial velocity dispersions. The best-fit model velocity ellipsoid axis ratio is $\sigma_z/\sigma_R = 0.25 \pm 0.20$.

4.2 NGC 3810

The photometric data for NGC 3810 (see §2.2) indicates that the disk light should dominate beyond $R > 5$ arcsec in the Sc galaxy NGC 3810. However, at these radii the measured velocity dispersions are not consistent with a stellar disk but instead hint at the presence of a (hidden) stellar bar. This is particularly apparent along the major axis at negative radii where the velocity dispersion profile is flat out to 8 arcsec. To avoid the contaminating effect of a potential stellar bar on velocity ellipsoid modelling we conservatively exclude all kinematic data at radii less than 10 arcsec. While this limits the dataset, its final size and quality are similar to that of the NGC 2280 dataset. The best-fit model velocity ellipsoid axis ratio is $\sigma_z/\sigma_R = 0.29 \pm 0.12$.

4.3 The Velocity Ellipsoid in Spiral Galaxies

Combining these measurements of σ_z/σ_R for late-type galaxies with our results for earlier-type spirals (Gerssen et al. 1997, 2000; Shapiro et al. 2003), we probe the shape of the velocity ellipsoid over the full extent of the

Hubble sequence of disk galaxies. The results are shown in Figure 4 and reveal a clear trend in σ_z/σ_R with morphological type. The combined data are best fit by a line with slope -0.12 ± 0.05 , with a 0.1% probability of no correlation. The addition of our new results in late-type galaxies confirm and strengthen the trend identified at much lower significance by Gerssen et al. (2000) and Shapiro et al. (2003).

We include in the data and linear regression in Figure 4 the Hipparcos value for the velocity ellipsoid in the solar neighbourhood (0.53 ± 0.07 , Dehnen & Binney 1998), which is consistent with results based on the RAVE data (0.55, Casetti-Dinescu et al. 2011, but see also Veltz et al. 2008). This measurement is obtained at the solar radius (at $\sim 2-3$ scale lengths in the Milky Way) and is therefore comparable to our measurements in external galaxies, radially averaged in each galaxy over a typical range of $\sim 1-3$ disk scale lengths.

Using a different technique, van der Kruit & de Grijs (1999) did not observe a clear trend in velocity ellipsoid ratio in galaxies of Hubble type Sb to Scd. However, their results are statistical (the rms of determinations for multiple edge-on galaxies of the same type) and based on photometry only. An advance of this technique combines photometry and spectra of edge-on galaxies to measure the quantity $\sqrt{M/L}(\sigma_R/\sigma_z)^{-1}$; assumptions of universal mass-to-light (M/L) ratios and/or Toomre Q parameters in late-type spirals can then be used to estimate the velocity ellipsoid ratio (Kregel et al. 2005). For their sample of 15 edge-on galaxies of Hubble types Sb to Scd, these authors obtained a range of estimates of σ_z/σ_R consistent with our direct measurements and following a marginal trend with Hubble type.

A promising step forward is the use of integral field

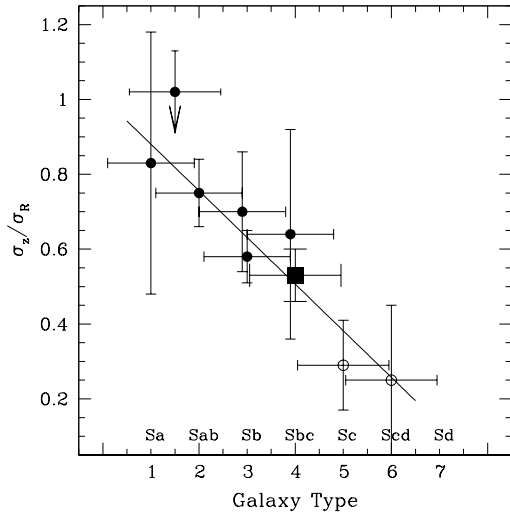


Figure 4. Velocity ellipsoid ratio σ_z/σ_R as a function of galactic type (Hubble stage T). The solid points show the results that we obtained previously (Shapiro et al. 2003). The results that we derive in this paper for two late type spirals are shown as the open circles. Horizontal errors represent the uncertainty inherent in galaxy classification (Naim et al. 1995). The filled square is the value in the Solar Neighbourhood derived from Hipparcos data (Dehnen & Binney 1998).

units (IFUs) to observe velocity dispersions in disk galaxies. This is observationally more efficient than obtaining long-slit spectra, one at a time, along two (or more) position angles. Additionally, since IFUs uniformly sample velocity dispersions along both azimuth and radius across the disk, the assumption of the epicycle approximation, employed here for long-slit data, can be relaxed. Noordermeer et al. (2008) use the PPAK IFU to explore velocity dispersions in disk galaxies and to constrain the shape of the velocity ellipsoid in one system, NGC 2985. Their measurement of $\sigma_z/\sigma_R \approx 0.7$ is consistent with our previous result for this system (0.75 ± 0.09 ; Gerssen et al. 2000) and confirms that the epicycle theory we assume is indeed applicable in this galaxy.

In a series of conference proceedings Westfall et al. (2008, 2010) present their ongoing work with the SparsePAK and PPAK IFUs to constrain the velocity ellipsoid shape and its radial variation in a sample of spiral galaxies. These authors find a strong dependence on their modelled velocity ellipsoid shape with their measurement techniques and assumptions; they present and describe an analysis comparable to ours for a single galaxy, NGC 3982 (Sb), for which they find $\sigma_z/\sigma_R = 0.31 - 0.73$ over a radial range of 1 – 2 photometric scalelengths, broadly consistent with our results for galaxies of similar Hubble type. These authors also find some evidence for variation in the velocity ellipsoid ratio with radius, indicating the potential of IFU data in future studies of the velocity ellipsoid in external galaxies.

4.4 The Velocity Ellipsoid across the Hubble Sequence

The SAURON team has used the IFU of the same name to study the kinematics of elliptical and lenticular galaxies and have shown that many early-type galaxies, the so-called

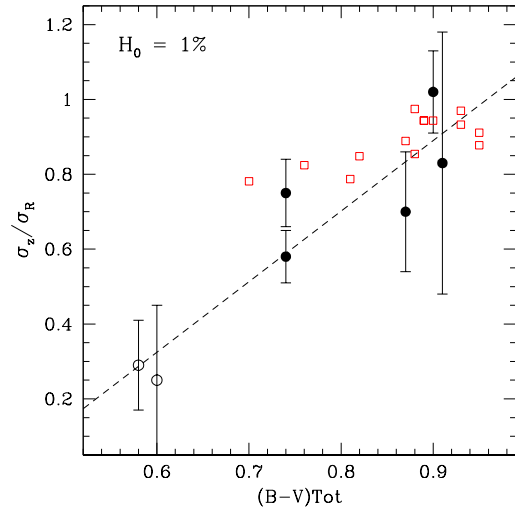


Figure 5. Velocity ellipsoid ratio σ_z/σ_R as a function of inclination- and extinction-corrected galaxy colour (available in HyperLeda for 7 of our 8 spirals and the fast-rotating E/S0s). The black points indicate our spiral galaxy data, and the red squares are the data of Cappellari et al. (2007) for fast-rotating E and S0 galaxies. The linear fit (dashed line) is to the spiral galaxies only. The probability of no correlation, null hypothesis H_0 , is one percent.

“fast rotators,” are bulge-dominated galaxies that nevertheless contain a significant disk component (Kuntschner et al. 2006; Krajnović et al. 2008). It is therefore interesting to investigate how the disks of these early-type galaxies are related to those in spiral galaxies.

Cappellari et al. (2007) have used axisymmetric Schwarzschild dynamical models to extract the three-dimensional orbital structure of a subsample of the SAURON galaxies and measure the shape of their velocity ellipsoids. These anisotropy measurements are luminosity-weighted, giving more weight to the high-density equatorial plane, and volume-averaged, giving more weight to larger radii; as a result, the global anisotropies (see table 2 of Cappellari et al. 2007) are dominated by the disks and are therefore comparable to our measurements in later-type galaxies (Cappellari et al. private communication). Since Hubble T-type is less meaningful in early-type galaxies than in spirals, we cannot add these points directly to Figure 4. Instead we use galaxy $B - V$ colour as a proxy for morphological type and plot this quantity against σ_z/σ_R in Figure 5 for both the SAURON sample and our sample of spiral galaxies. Colours are taken from HyperLeda² and are listed for our sample in Table 4.

The combined data span the Hubble sequence from E to Scd and show the strong correlation between velocity ellipsoid ratio and galaxy colour, as expected from Figure 4, given the known relationship between galaxy colour and Hubble type. In Figure 5, we find a continuous trend of increasing anisotropy in bluer galaxies. Moreover, we find that the anisotropies of the E/S0 galaxies overlap with those of the earliest-type spirals in our sample. However, in the bluest

² <http://leda.univ-lyon1.fr/>

range ($B - V \approx 0.7 - 0.8$) of the overlapping data, there is some evidence that elliptical and lenticular fast rotators are preferentially more isotropic than their spiral cousins.

5 DISCUSSION

5.1 Dependence of the Velocity Ellipsoid Shape on Galaxy Properties

Figures 4 and 5 point to a deep connection between galaxy-wide properties and axial ratio of the stellar velocity ellipsoid in the galaxy disk. In this and the following sections, we examine the source of these relationships.

The tighter of the two correlations is that between galaxy morphology, parameterized through Hubble T-type, and the shape of the velocity ellipsoid (Figure 4). However, as a semi-quantitative descriptor of galaxies, T-type is a somewhat subjective property based on several qualitative criteria that are largely but not perfectly correlated. In the de Vaucouleurs RC3 classification used here, these criteria are the bulge-to-disk ratio and the tightness of the spiral structure. Moreover, a number of additional galaxy properties not directly involved in the determination of T-type also correlate with morphology, such that earlier-type spirals tend to have higher masses, higher stellar mass surface densities, redder colours, and lower gas fractions than their late-type counterparts, albeit with large scatter (see e.g. Roberts & Haynes 1994).

It is therefore not straightforward to determine which of the fundamental galaxy properties that correlate with T-type drive the relation in Figures 4 and 5. Broadly, these properties fall into two general categories: (1) structural properties related to the large-scale evolutionary history of a galaxy such as galaxy mass and relative prominence of the bulge, and (2) properties related to past, current, and future star formation processes such as galaxy colour, tightness of the spiral structure, and gas fraction. The interesting result from Figure 4 is that one or both of these aspects of a galaxy’s evolution is intimately related to the heating of its disk.

Moreover, Figure 5 reveals that these same processes are also at work in fast-rotating early-type galaxies. The more isotropic shape of the velocity ellipsoid in early-types, relative to late-types with similar colours, may indicate a difference in disk heating mechanisms at work in early- and late-type galaxies. One possibility is a difference in strength of a particular mechanism; another is that an additional heating agent may need to be invoked.

5.2 Disentangling Disk Heating Agents

Of the numerous theoretically studied disk heating agents (see § 1), each is expected to behave differently in the vertical and radial directions as a function of galaxy morphology. To constrain the nature of these agents in our spiral galaxies, we therefore examine the individual axes of the velocity ellipsoid in our galaxy sample. (The evolution of the velocity ellipsoid in the SAURON sample of elliptical and lenticular galaxies is an equally interesting problem beyond the scope of this paper, and we do not discuss it further.)

Using the exponential parametrization of σ_z and σ_R

with radius (§ 3.2), we evaluate the magnitude of the dispersion at half the measured kinematic scale length, $h_{kin}/2$. This radius falls within the range constrained by the observations for all but one of our eight galaxies. The local isothermal approximation of stellar disks predicts that $h_{kin}/2 \approx h_{phot}$ (e.g. van der Kruit & Freeman 1986; Martinsson 2011). Our measurements of h_{kin} are broadly consistent with this prediction, albeit with large scatter and noticeable outliers.

The relationship of the magnitudes of the dispersions at $h_{kin}/2$ to each other and to the shape of the velocity ellipsoid is shown in Figure 6. In this figure, the tightest trend, with a 1% probability of no correlation, is between the magnitude of the vertical velocity dispersions σ_z and the shape of the velocity ellipsoid σ_z/σ_R ; in stark contrast, there is no correlation between σ_z/σ_R and the magnitude of the radial velocity dispersions σ_R . Although there is evidence for a relationship between σ_z and σ_R , a constant ratio (i.e. linear fit) is inconsistent with our direct measurements of variations in σ_z/σ_R among galaxies and cannot be the best description of the data. In the left panel of Figure 6, we therefore plot the prediction for the relationship between σ_z and σ_R based on the observed linear correlation between σ_z and σ_z/σ_R in the middle panel. The projection of the σ_z - σ_z/σ_R correlation into the (σ_z, σ_R) parameter space is shown as the dashed line. The uncertainty in this projection is shown by the shaded area, bounded by the 1σ uncertainties on the linear fit and by the line where $\sigma_z/\sigma_R = 1$. Within the scatter, the predicted relationship between σ_z and σ_R matches the data.

These results are a powerful new tool in probing the nature of disk heating agents at work across the Hubble sequence, and they demonstrate the feasibility of observationally disentangling disk heating agents in spiral galaxies. In particular, Figure 6 places two important constraints on disk heating mechanisms:

(1) There is a disk heating agent that is responsible for increasing both vertical and radial dispersions, which we call the “three-dimensional agent.” The trend of σ_z with σ_R demonstrates that, in external galaxies, both dispersion components grow simultaneously although not at the same rate, as is also observed in the solar neighbourhood (e.g. Holmberg et al. 2007). The tight correlation between σ_z and σ_z/σ_R additionally requires that the three-dimensional agent responsible for the magnitude of the vertical dispersions also determine the shape of the velocity ellipsoid, such that larger vertical dispersions are coincident with more isotropic heating and smaller vertical dispersions are coincident with more radially anisotropic heating. The correlations in Figures 4 and 6 therefore imply that the strength of the three-dimensional agent in a galaxy should correlate strongly with σ_z , σ_z/σ_R , and the galaxy properties associated with T-type and correlate weakly with σ_R .

(2) It is likely, given the observed scatter in the σ_z - σ_R relation, that there is also a second agent involved in radial heating, which we call the “radial agent.” The lack of correlation between σ_R and σ_z/σ_R suggests that this heating mechanism has no effect on the vertical dispersions (and therefore on the shape of the velocity ellipsoid) and operates only in the plane of the galaxy. Additionally, the lack of correlation between σ_R and σ_z/σ_R implies that the presence or strength of the radial agent in a galaxy should correlate only

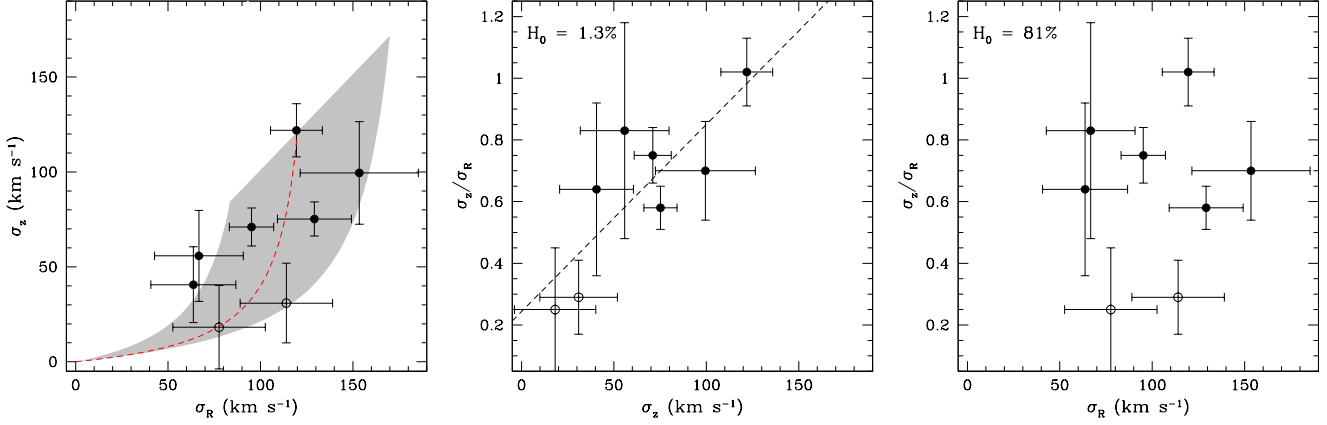


Figure 6. Correlations between the velocity ellipsoid magnitudes and shapes for all eight galaxies in our sample. Here and in the following figures, H_0 denotes the probability of the null hypothesis, i.e. that there is no correlation. **Left panel:** The vertical ellipsoid magnitudes as a function of the radial component magnitude. The dashed line is the projection of the best-fit correlation in the middle panel, see text. The shaded area is bounded by the one-sigma uncertainty on the projected correlation and by the line $\sigma_z/\sigma_R = 1$. **Middle panel:** The shape of the velocity ellipsoid for each galaxy in our sample plotted as a function of the vertical dispersion magnitude. The results are tightly correlated, dashed line. **Right panel:** The velocity ellipsoid shape as a function of the radial dispersion magnitude. There appears to be no relation.

Table 4. Properties of disk galaxies with velocity ellipsoid shape and magnitude measurements.

Galaxy	Hubble Type	D (Mpc)	σ_z/σ_R	(B-V)Tot	Σ_{H_2} (M_\odot/pc^{-2})	Arm Class
NGC 2460	Sa	20	0.83 ± 0.35	0.91	...	12
NGC 2775	Sa/Sab	19	$<1.02 \pm 0.11$	0.90	33 ± 6	3
NGC 2985	Sab	18	0.75 ± 0.09	0.74	21 ± 7	3
NGC 488	Sb	30	0.70 ± 0.16	0.87	25 ± 6	3
NGC 1068	Sb	16	0.58 ± 0.07	0.74	41 ± 14	3
NGC 4030	Sbc	21	0.64 ± 0.28	...	16 ± 3	9
NGC 3810	Sc	14	0.29 ± 0.12	0.58	28 ± 6	2
NGC 2280	Scd	26	0.25 ± 0.20	0.60	...	9

- 1) Hubble classifications are from NED.
- 2) Distances are derived from the redshift values listed in NED and assuming a Hubble constant of 73 km/s/Mpc.
- 3) Colours are from HyperLeda.
- 4) Arm Class values are from Elmegreen & Elmegreen (1987).

with σ_R , and not with σ_z , σ_z/σ_R , or the galaxy properties associated with T-type.

Two of the most commonly invoked disk heating agents are GMCs and transient spiral structure (§ 1), with the former expected to operate in three dimensions and the latter only in the plane of the disk. In Sections 5.3 and 5.4, we investigate whether these heating mechanisms are consistent with our observational constraints on the three-dimensional agent and radial agent, respectively.

5.3 GMCs as a Heating Agent

We estimate the molecular gas surface mass densities for six of the eight galaxies in our sample for which the CO models of Young et al. (1995) are available. We compute Σ_{H_2} in each system as the average surface density over the same range in radii used in our velocity ellipsoid measurements. The results, with rather large error bars, are tabulated in Table 4.

In Figure 7, the velocity ellipsoid shape and magnitude

are shown as a function of Σ_{H_2} . If molecular gas is the dominant “three-dimensional agent”, we expect the gas surface density to correlate with σ_z , σ_R (weakly), σ_z/σ_R , and T-type. The radial dispersion shown in the right panel are indeed consistent with the expected increase in dispersions with gas surface density; however, a trend is not evident in the vertical dispersions (middle panel). The probability that neither radial nor vertical dispersions are correlated with surface density is 19% and 44%, respectively. Moreover, Σ_{H_2} is also not correlated with the velocity ellipsoid shape σ_z/σ_R and is instead consistent with scattering around a constant value. Roberts & Haynes 1994 show that the surface density of molecular gas increases with Hubble T-type, although this trend is not clearly reflected in our much smaller sample (not shown). Together, these relationships point to GMCs as only marginally consistent with being the three-dimensional agent.

Theoretically, three-dimensional heating via GMCs has been shown to drive the velocity ellipsoid axis ratio from an initially isotropic distribution to a small equilibrium value

(e.g. Jenkins & Binney 1990). Interestingly, Sellwood (2008) argued that this mechanism alone can explain the observed disk heating in the Milky Way, with the degree of anisotropy in the distribution of the scattering events determining the final equilibrium ratio σ_z/σ_R . However, our observed variation in σ_z/σ_R with T-type in external galaxies is larger than can be comfortably explained with GMCs as the only heating mechanism.

The identification of GMCs as the three-dimensional heating agent is not straightforward. GMCs are consistent with the behavior required by the data but leave room for alternative explanations. Jenkins (1992) likewise notes that the observations of constant disk scale height with radius in external galaxies is difficult to reconcile with the observed exponential distribution of molecular clouds if GMCs are important disk heating agents. Other potential three-dimensional agents include transient asymmetric spiral structure, dark halo objects (black holes and dark matter substructure), globular clusters, and accreting satellite galaxies (Saha et al. 2010; Lacey & Ostriker 1985; Hänninen & Flynn 2002; Vande Putte et al. 2009; Velazquez & White 1999). Of these, numerical simulations have demonstrated that dark halo objects and globular clusters are unlikely to exist in sufficient numbers to produce the observed heating (Lacey & Ostriker 1985; Hänninen & Flynn 2002; Vande Putte et al. 2009; Benson et al. 2004), leaving spiral structure and accreting satellites as viable mechanisms. It is not obvious how the accretion history of a galaxy might be quantified and subsequently compared to the observed shape of the velocity ellipsoid, so observational tests of the viability of this alternative heating mechanism are not straightforward. In contrast, spiral structure is a direct observable, and we examine the effects of this potential heating agent in the following section.

5.4 Spiral Structure as a Heating Agent

To investigate the role of spiral structure on disk heating we use the arm class parameter, developed by Elmegreen & Elmegreen (1987), to quantify the strength and symmetry of the spiral structure in galaxies. They define this parameter to describe the orderliness of spiral structure from flocculent (class 1) to grand-design (class 12). The arm class parameters for our sample are listed in Table 4.

We compare the velocity ellipsoid shape and magnitudes in our sample galaxies to their arm classes in Figure 8 and find a strong correlation between σ_R and arm class. This can be interpreted as spiral structure preferentially forming in Toomre unstable disks (Toomre Q stability criterion; Toomre 1964). The Toomre Q is proportional to σ_R , such that larger velocity dispersions create more stable systems, which are then less responsive to the formation of (transient) spiral structure (e.g. Binney 2012). In our sample, we indeed find the most clear spiral structure (class 12) in those galaxies with the lowest σ_R .

In Figure 8, there is a marginal relationship between σ_z and spiral structure at much lower significance than that with σ_R , and no trend is evident between σ_z/σ_R and arm class. This latter result is consistent with the absence of a trend between arm class and T-type found by Elmegreen & Elmegreen (1987) and confirmed in our much

smaller sample (not shown). Spiral structure thus correlates primarily with σ_R , weakly (if at all) with σ_z , and not with σ_z/σ_R nor T-type. Based on the requirements of different heating agents described in Section 5.2, spiral transients are excellent candidates for the “radial agent”.

6 CONCLUSIONS

In this paper, we present the kinematics and modelled velocity ellipsoid shape, i.e. the ratio of the vertical and radial velocity dispersions σ_z/σ_R , in two late-type disk galaxies, NGC 2280 (Scd) and NGC 3810 (Sc). Combining these results with our previous measurements of this ratio in six early type disks demonstrates that the shape of the velocity ellipsoid is strongly correlated with Hubble type and with galaxy color. Moreover, early-type galaxies (E/S0) with significant disk components appear to follow a related trend.

Examination of the relationship of vertical and radial dispersions (σ_z and σ_R) with each other and with σ_z/σ_R shows that σ_z/σ_R correlates strongly with σ_z but not at all with σ_R . This suggests that kinematic observations alone can disentangle the effects of disk heating mechanisms that act in three-dimensions from the effects of those that act predominantly in the plane of the disk.

Two commonly invoked disk heating mechanisms are stellar scattering off of giant molecular clouds (as the three-dimensional agent) and perturbations from transient spiral structure (as the radial agent). To test the applicability of these theories to our data across the full range of morphological types, we probe the relationship of molecular gas surface mass density and of spiral arm structure to our observed dispersions (σ_z and σ_R) and their ratio (σ_z/σ_R). The data show that spiral structure varies between galaxies exactly as expected of the radial heating agent, and therefore it seems likely that spiral structure is responsible for (morphologically-independent) heating in the plane of galactic disks. The data are tentatively consistent with GMCs being the three-dimensional agent, although the gap between the expected and observed variation between galaxies for the three-dimensional agent leaves room for alternative interpretations.

These results suggest exciting possibilities for future work in directly probing disk heating agents in external galaxies. Open questions include the nature of the three-dimensional agent and its relationship to the molecular content of galaxies, the possible relationship of stellar populations to disk heating mechanisms, and the relationship of disk heating mechanisms in fast-rotating early-type galaxies to those of spirals.

ACKNOWLEDGMENTS

We thank the staff of the La Silla Observatory, in particular Emanuela Pompei, for their outstanding support during our observing runs. This paper also benefited significantly from discussions with Anne-Marie Weijmans, Cecilia Scannapieco, Ivan Minchev and Jesús Falcón Barroso. We also thank the referee for helpful comments. KSG wishes to acknowledge the Sigma Xi Grant in Aid of Research for travel support that enabled the observations presented

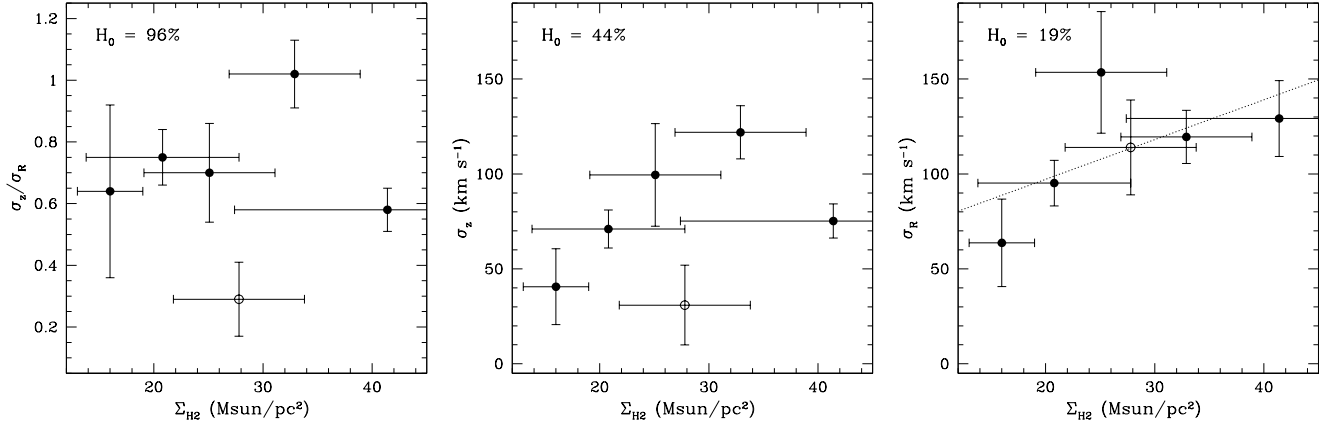


Figure 7. The velocity ellipsoid shape and magnitudes as a function of the H_2 gas surface density. Gas densities are estimated from the CO measurements of Young et al. (1995) and are computed as average values over the radii used in our kinematic analysis. **Left:** The velocity ellipsoid shapes are not correlated with the molecular gas surface density. **Middle:** There is a hint that the vertical component of the velocity dispersion is correlated with Σ_{H_2} , but the scatter is too large to state this conclusively. **Right:** The radial component increases with molecular gas density.

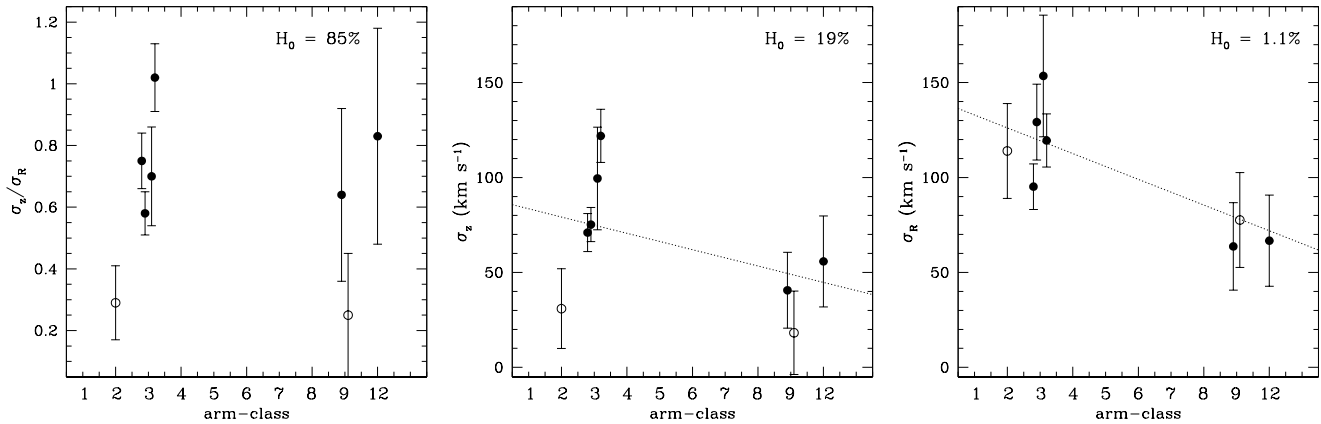


Figure 8. The velocity ellipsoid shape and magnitudes as a function of arm class, as defined in Elmegreen & Elmegreen (1987) to quantify the orderliness of spiral structure from flocculent (class 1) to grand-design (class 12). Note that there is no arm-class 10 and 11 (cf., Figure 1 in Elmegreen & Elmegreen 1987). **Left:** The velocity ellipsoid shape is not correlated with arm class. **Middle:** The vertical magnitude of the ellipsoid decreases with arm class. **Right:** There is a clear trend between arm class and radial component, as expected from the Toomre Q criterion, see text. Note that for plotting purposes we have added small offsets to galaxies with the same arm class.

here. This research has made use of the Hyperleda database (<http://leda.univ-lyon1.fr>) and of the NASA/IPAC Extragalactic Database, which is operated by the Jet Propulsion Laboratory, California Institute of Technology, under contract with the National Aeronautics and Space Administration.

REFERENCES

- Barbanis B., Woltjer L., 1967, *ApJ*, 150, 461
 Benson A. J., Lacey C. G., Frenk C. S., Baugh C. M., Cole S., 2004, *MNRAS*, 351, 1215
 Binney J., 2012, *ArXiv e-prints*
 Binney J., Dehnen W., Bertelli G., 2000, *MNRAS*, 318, 658
 Cappellari M., Emsellem E., 2004, *PASP*, 116, 138
 Cappellari M., Emsellem E., Bacon R., Bureau M., Davies R. L., de Zeeuw P. T., Falcón-Barroso J., Krajnović D., Kuntschner H., McDermid R. M., Peletier R. F., Sarzi M., van den Bosch R. C. E., van de Ven G., 2007, *MNRAS*, 379, 418
 Carlberg R. G., Dawson P. C., Hsu T., Vandenberg D. A., 1985, *ApJ*, 294, 674
 Casetti-Dinescu D. I., Girard T. M., Korchagin V. I., van Altena W. F., 2011, *ApJ*, 728, 7
 Comerón S., Knapen J. H., Beckman J. E., 2008, *A&A*, 485, 695
 Dehnen W., Binney J. J., 1998, *MNRAS*, 298, 387
 Driver S. P., Allen P. D., Liske J., Graham A. W., 2007, *ApJ*, 657, L85
 Elmegreen D. M., Elmegreen B. G., 1987, *ApJ*, 314, 3
 Eskridge P. B., Frogel J. A., Pogge R. W., Quillen A. C., Berlind A. A., Davies R. L., DePoy D. L., Gilbert K. M., Houdashelt M. L., Kuchinski L. E., Ramírez S. V., Sellgren K., Stutz A., Terndrup D. M., Tiede G. P., 2002,

- ApJS, 143, 73
- Fuchs B., 2001, MNRAS, 325, 1637
- Gerssen J., Kuijken K., Merrifield M. R., 1997, MNRAS, 288, 618
- Gerssen J., Kuijken K., Merrifield M. R., 2000, MNRAS, 317, 545
- Gerssen J., Kuijken K., Merrifield M. R., 2003, MNRAS, 345, 261
- Hänninen J., Flynn C., 2002, MNRAS, 337, 731
- Holmberg J., Nordström B., Andersen J., 2007, A&A, 475, 519
- Jenkins A., 1992, MNRAS, 257, 620
- Jenkins A., Binney J., 1990, MNRAS, 245, 305
- Kassin S. A., de Jong R. S., Pogge R. W., 2006, ApJS, 162, 80
- Knapen J. H., de Jong R. S., Stedman S., Bramich D. M., 2003, MNRAS, 344, 527
- Krajnović D., Bacon R., Cappellari M., Davies R. L., de Zeeuw P. T., Emsellem E., Falcón-Barroso J., Kuntschner H., McDermid R. M., Peletier R. F., Sarzi M., van den Bosch R. C. E., van de Ven G., 2008, MNRAS, 390, 93
- Kregel M., van der Kruit P. C., Freeman K. C., 2005, MNRAS, 358, 503
- Kroupa P., 2002, MNRAS, 330, 707
- Kuntschner H., Emsellem E., Bacon R., Bureau M., Cappellari M., Davies R. L., de Zeeuw P. T., Falcón-Barroso J., Krajnović D., McDermid R. M., Peletier R. F., Sarzi M., 2006, MNRAS, 369, 497
- Lacey C. G., 1984, MNRAS, 208, 687
- Lacey C. G., Ostriker J. P., 1985, ApJ, 299, 633
- Martinsson T., 2011, PhD thesis, University of Groningen
- Minchev I., Quillen A. C., 2006, MNRAS, 368, 623
- Naim A., Lahav O., Buta R. J., Corwin Jr. H. G., de Vaucouleurs G., Dressler A., Huchra J. P., van den Bergh S., Raychaudhury S., Sodre Jr. L., Storrie-Lombardi M. C., 1995, MNRAS, 274, 1107
- Noordermeer E., Merrifield M. R., Aragón-Salamanca A., 2008, MNRAS, 388, 1381
- Nordström B., Mayor M., Andersen J., Holmberg J., Pont F., Jørgensen B. R., Olsen E. H., Udry S., Mowlavi N., 2004, A&A, 418, 989
- Press W. H., Teukolsky S. A., Vetterling W. T., Flannery B. P., 1992, Numerical recipes in FORTRAN. The art of scientific computing
- Prieto M., Aguerri J. A. L., Varela A. M., Muñoz-Tuñón C., 2001, A&A, 367, 405
- Quillen A. C., Garnett D. R., 2001, in J. G. Funes & E. M. Corsini ed., Galaxy Disks and Disk Galaxies Vol. 230 of Astronomical Society of the Pacific Conference Series, The Saturation of Disk Heating in the Solar Neighborhood and Evidence for a Merger 9 Gyr Ago. pp 87–88
- Roberts M. S., Haynes M. P., 1994, ARAA, 32, 115
- Saha K., Tseng Y.-H., Taam R. E., 2010, ApJ, 721, 1878
- Scannapieco C., Gadotti D. A., Jonsson P., White S. D. M., 2010, MNRAS, 407, L41
- Scannapieco C., White S. D. M., Springel V., Tissera P. B., 2011, MNRAS, 417, 154
- Schwarzschild K., 1907, Göttingen Nachrichten, p. 614
- Seabroke G. M., Gilmore G., 2007, MNRAS, 380, 1348
- Sellwood J. A., 2008, in J. G. Funes & E. M. Corsini ed., Formation and Evolution of Galaxy Disks Vol. 396 of Astronomical Society of the Pacific Conference Series, Dynamical Evolution of Disk Galaxies. p. 241
- Shapiro K. L., Gerssen J., van der Marel R. P., 2003, AJ, 126, 2707
- Soubiran C., Bienaymé O., Mishenina T. V., Kovtyukh V. V., 2008, A&A, 480, 91
- Spitzer Jr. L., Schwarzschild M., 1951, ApJ, 114, 385
- Toomre A., 1964, ApJ, 139, 1217
- van der Kruit P. C., de Grijs R., 1999, A&A, 352, 129
- van der Kruit P. C., Freeman K. C., 1986, ApJ, 303, 556
- Vande Putte D., Cropper M., Ferreras I., 2009, MNRAS, 397, 1587
- Velazquez H., White S. D. M., 1999, MNRAS, 304, 254
- Veltz L., Bienaymé O., Freeman K. C., Binney J., Bland-Hawthorn J., Gibson B. K., Gilmore G., et al. 2008, A&A, 480, 753
- Weijmans A.-M., Cappellari M., Bacon R., de Zeeuw P. T., Emsellem E., Falcón-Barroso J., Kuntschner H., McDermid R. M., van den Bosch R. C. E., van de Ven G., 2009, MNRAS, 398, 561
- Weinzirl T., Jogee S., Khochfar S., Burkert A., Kormendy J., 2009, ApJ, 696, 411
- Westfall K. B., Bershadsky M. A., Verheijen M. A. W., Andersen D. R., Swaters R. A., 2008, in J. G. Funes & E. M. Corsini ed., Formation and Evolution of Galaxy Disks Vol. 396 of Astronomical Society of the Pacific Conference Series, Deconstructing Disk Velocity Distribution Functions in the Disk-Mass Survey. p. 41
- Westfall K. B., Bershadsky M. A., Verheijen M. A. W., Martinsson T. P. K., Andersen D. R., Swaters R. A., 2010, in V. P. Debattista & C. C. Popescu ed., American Institute of Physics Conference Series Vol. 1240 of American Institute of Physics Conference Series, Galaxy Physics via the Disk Stellar Velocity Ellipsoid. pp 429–430
- Wielen R., 1977, A&A, 60, 263
- Young J. S., Xie S., Tacconi L., Knezek P., Viscuso P., Tacconi-Garman L., Scoville N., Schneider S., Schloerb F. P., Lord S., Lesser A., Kenney J., Huang Y.-L., Devoreux N., Claussen M., Case J., Carpenter J., Berry M., Allen L., 1995, ApJS, 98, 219